

Research paper

Malvidin promotes PGC-1 α /Nrf2 signaling to attenuate the inflammatory response and restore mitochondrial activity in septic acute kidney injury

Hui Fan^{a,b,1}, Yong Sun^{a,1}, Xiao Zhang^{a,b}, Yao Xu^a, Yuanyuan Ming^a, Le Zhang^a, Panpan Zhao^{a,*}

^a Institute of Neuroscience, Neurosurgery Department, The First People's Hospital of Lianyungang, Lianyungang, 222000, China

^b Jiangsu Key Laboratory of Marine Pharmaceutical Compound Screening, College of Pharmacy, Jiangsu Ocean University, Lianyungang, 222005, China

ARTICLE INFO

Keywords:

Sepsis

NLRP3

Oxidative stress

Mitochondrial biogenesis

Acute kidney injury

ABSTRACT

Acute kidney injury (AKI) in sepsis is a vital and dangerous organ failure caused by an infection-induced dysregulation of the host reaction. Malvidin possesses significant anti-inflammatory and antioxidant bioactivities. This study explored the critical roles of malvidin in sepsis AKI and the crosstalk among mitochondrial function, nucleotide-binding oligomerization-like receptor 3 (NLRP3) inflammasome and nuclear factor erythroid 2 (Nrf2) signaling pathway. First, C57BL/6 mice were administered lipopolysaccharide intraperitoneally for 6 h to create an AKI model of sepsis. Hematoxylin-eosin staining and serum biomarker assays showed that malvidin protected from AKI in sepsis. *Real-time fluorescence quantitative polymerase chain reaction* analysis revealed that malvidin was able to inhibit inflammatory cytokines and mediators. Western blot assays indicated that malvidin suppressed NLRP3 inflammasome activation and enhanced antioxidant properties. Additionally, human renal tubular epithelial cells were stimulated by lipopolysaccharide/adenosine triphosphate to establish an NLRP3 inflammasome activation model *in vitro*, and in line with findings *in vivo*, malvidin significantly inhibited NLRP3 inflammasome activation. Furthermore, our data indicate that malvidin restored mitochondrial quality and function, reduced reactive oxygen species production, increased mitochondrial membrane potential, enhanced mitochondrial DNA copy number, and promoted peroxisome proliferator-activated receptor gamma coactivator 1- α (PGC-1 α) nuclear translocation. Moreover, inhibitor blockade assays indicated that both PGC-1 α and Nrf2 affected the inhibition of the NLRP3 inflammasome by malvidin. Finally, immunoprecipitation assays showed that malvidin promoted PGC-1 α and Nrf2 interactions. Overall, malvidin alleviated lipopolysaccharide-induced sepsis AKI, improved mitochondrial function and mitochondrial biogenesis, and inhibited the NLRP3 inflammasome through the PGC-1 α /Nrf2 signaling pathway, suggesting that malvidin might translate into clinical applications for sepsis AKI therapy.

1. Introduction

Acute kidney injury (AKI) caused by sepsis, accompanied by systemic inflammation, is a serious threat to human health. Currently, many treatments for sepsis are in the clinical trial stage, so it is necessary to continue to explore reagents of natural origin for the treatment of AKI in sepsis.

When sepsis occurs, the intrinsic immune system first acts to release inflammatory mediators and clear exogenous pathogens. Lipopolysaccharide (LPS) is the main virulence component of gram-negative bacteria and is one of the recognized pathogen-associated molecular

patterns (PAMPs) of sepsis, activating the nucleotide-binding oligomerization-like receptor 3 (NLRP3) inflammasome [1]. During sepsis, because of the inhibition of mitochondrial oxidative phosphorylation and constant inflammatory stimuli such as interleukin-6 (IL-6) and tumor necrosis factor- α (TNF- α), a large amount of reactive oxygen species (ROS) accumulate in the body, which induces an imbalance in oxidative and antioxidant systems, resulting in disturbed cellular metabolism and thus tissue damage [2]. As a category of systemic inflammatory diseases, the dynamic change from pro-inflammatory to immunosuppressive during the development of sepsis may be reflected in the NLRP3 inflammasome [3]. Therefore, the suppression of the

* Corresponding author.

E-mail address: zhaopp19@mails.jlu.edu.cn (P. Zhao).

¹ These authors have contributed equally to this work and share first authorship.

NLRP3 inflammasome is a potential therapeutic target in septic AKI. Additionally, it has been reported that enhanced antioxidant protein nuclear factor erythroid 2 (Nrf2) could inhibit NLRP3 inflammasome activation [4,5].

Mitochondria are abundant in kidney tubular epithelial cells. Persistent mitochondrial dysfunction leads to a poor prognosis for AKI [6]. Mitochondrial quality control maintains mitochondrial homeostasis in the body according to mitochondrial fusion/division, mitochondrial autophagy and mitochondrial biogenesis. Peroxisome proliferator-activated receptor gamma coactivator-1 α (PGC-1 α), a key modulator of mitochondrial biogenesis, acts on the downstream nuclear respiration elements Nrf1 and Nrf2 and then activates mitochondrial transcription factor A (TFAM), combining with the respiratory chain complex subunit, thereby upregulating mtDNA replication and transcription [7,8]. Previous studies revealed that PGC-1 α inhibited NLRP3 inflammasome activation [9,10]. Therefore, the search for natural agents that target mitochondrial biogenesis may become an effective strategy for the treatment of AKI in sepsis.

Malvidin (Mv), a type of anthocyanin, is commonly found in natural foods of blue, purple, and red hues, such as grapes, blueberries, and black currants. It serves as a natural pigment and possesses antioxidant properties, demonstrating a variety of pharmacological effects, including anti-inflammatory and antioxidative actions [11–14]. As an effective antioxidant, Mv helps neutralize harmful free radicals, reducing oxidative stress and thereby aiding in the prevention of cellular damage. Its derivatives have been shown to inhibit the production of ROS and the accumulation of malondialdehyde (MDA), while enhancing glutathione peroxidase (GSH-PX) activity and superoxide dismutase (SOD) levels in cells treated with hydrogen peroxide [15]. Additionally, Mv's anti-inflammatory and antioxidative capabilities contribute to preventing stomach and duodenal ulcers [16], alleviating brain diseases associated with sepsis [17], and exhibiting various pharmacological properties such as anti-obesity, anti-diabetes, and anti-cancer effects [18]. However, these specific molecular mechanisms need to be investigated in depth. Here, we used models of LPS-induced AKI in sepsis in mice and LPS/adenosine triphosphate (ATP) costimulated the NLRP3 inflammasome in HK-2 cells, aiming to elucidate the protective roles of Mv in sepsis AKI and the regulatory mechanism of the PGC-1 α /Nrf2/NLRP3 signaling pathway, revealing the relationship between inflammation, oxidative stress and mitochondrial biogenesis and providing valuable targets for septic AKI therapies.

2. Materials and methods

2.1. Drugs and antibodies

Mv was available for purchase at Shanghai Yuanye Bio-Technology (CAS 643-84-5, molecular weight 366.75, purity $\geq 97\%$ by HPLC, Shanghai, China). LPS (0111: B4) and ATP were purchased from Sigma-Aldrich (MO, USA). NLRP3, PGC-1 α and IL-1 β were purchased from ABClonal Technology (Wuhan, China). Nrf2, HO-1, histone H3, GAPDH and HRP-labeled secondary antibodies were acquired from Proteintech (Wuhan). ASC was obtained from Wanleibio (Shenyang, China). The PGC-1 α inhibitor of SR18292 and Nrf2 inhibitor of ML385 were purchased from MedChemExpress (HY-19312, Monmouth Junction, NJ, USA).

2.2. Animal experimental design

Six weeks old male C57BL/6 mice were purchased from Eastern Breeding (Pizhou, China). All mice stayed in control circumstances for a week before the trials, which included unrestricted access to food and drink and a reasonable temperature ($25 \pm 2^\circ\text{C}$) and humidity ($55 \pm 15\%$). The National Research Council Guide for the Care and Use of Laboratory Animals and the Guidelines for Ethical Examination of Animal Welfare in China were followed throughout the animal experiment.

Additionally, all regulated operations are licensed through the Animal Ethical Council of Jiangsu Ocean University (permit code: 2020220611). Five groups of six mice each were created at random ($n = 6$): the normal group, LPS (10 mg/kg) group, Mv (low dose) + LPS group, Mv (medium dose) + LPS group and Mv (high dose) + LPS group. The doses from low to high are 5, 10 and 20 mg/kg body weight [14]. Mv was dissolved in dimethyl sulfoxide (DMSO) before use and injected through a single intraperitoneal (i.p.) injection at different doses 1 daily for 5 days. LPS was solubilized in 0.9 % NaCl solvent and injected via a single i.p. injection only once after the last dose of Mv. Six hours after LPS intraperitoneal injection [14], all mice were euthanized through carbon dioxide inhalation method for peritoneal macrophages, blood and kidney sample collection for subsequent assays.

2.3. Peritoneal macrophages collection and phenotyping

The mouse peritoneal cavity was washed with 12 mL of cold, sterile saline, and peritoneal fluid was collected from each experimental group. The peritoneal fluid was centrifuged at $300 \times g$ at room temperature for 5 min, followed by purification of peritoneal macrophages using an adherence selection method [19]. The expression levels of the M1-type pro-inflammatory cytokine IL-1 β and the M2-type anti-inflammatory cytokine arginase-1 (Arg-1) in macrophages were then measured respectively.

2.4. Histopathological analysis

Sections of kidney tissues were prepared for fixation in 4 % formaldehyde (Biosharp, Beijing, China) at room temperature. Specimens from 5 groups were encapsulated in paraffin, and then 4 μm slices were made. Hematoxylin-eosin (H&E) staining was applied to the slices, and typical microscope (Nikon DS-F12, Nikon, Japan) pictures were taken to further analyze kidney pathological abnormalities.

2.5. Biochemical index measurements

After blood collection from mouse eyes, the serum was acquired by centrifugation for 10 min at 3000 rpm at 4°C . Blood urea nitrogen (BUN) and creatinine (Cr) were tested on an automated chemistry machine (VITROS 4600, Johnson, America). Kidney tissue homogenate supernatant was analyzed for MDA, SOD, catalase (CAT) and GSH-PX activities according to the manufacturer's protocols by biochemical kits (Jiancheng Bioengineering, Nanjing, China). The MDA content was determined by the condensation of MDA with the substrate thiobarbituric acid, forming a red product, measured at an absorbance of 532 nm. SOD activity was determined by SOD's clearance of superoxide anion (O_2^-), inhibiting the formation of nitro blue tetrazolium, calculated by measuring absorbance at 450 nm. CAT decomposes H_2O_2 , and the remaining H_2O_2 reacts with ammonium molybdate. CAT activity was determined by measuring absorbance at 405 nm. GSH-PX promotes the reaction of H_2O_2 with GSH to form GSSG. The consumption of GSH was detected using dithiodinitrobenzoic acid, and GSH-PX activity was calculated by measuring GSH quantity through absorbance at 412 nm. Values were acquired at different absorbances using a microplate reader (Bioteck, Beijing, China).

2.6. RNA abstraction, complementary DNA (cDNA) synthesis, and real-time fluorescence quantitative polymerase chain reaction (RT-qPCR) analysis

With the use of TRIzol (Vazyme, Nanjing), RNA was acquired from kidney tissues. The quality or content was tested using a NanoDrop2000 spectrophotometer (Massachusetts, USA). Then, cDNA was generated using $5 \times \text{RTIV}$ all-in-one Mix (Monad, Wuhan). A Light Cycler® 480 (Roche, Shanghai, China) was selected for qPCR detection with SYBR Green Mix (Monad, Wuhan). Finally, the $2^{-\Delta\Delta\text{Ct}}$ method was employed

for mRNA quantification. The sequences of the primers are listed in [Supplementary Table S1](#).

2.7. Protein extraction and western blot assay

Human renal tubular epithelial cells HK-2 and kidney tissues were lysed with RIPA solution (Solarbio, Beijing) along with protease inhibitor (Sangon Biotech, Shanghai). After centrifugation at $12,000\times g$ at 4°C for 10 min, the homogenizing supernatants were acquired. Subsequently, protein concentrations were tested using a BCA kit (Biosharp).

To measure the protein level of cleaved caspase 1 (p20) in the cell culture supernatant, equivalent volumes of methanol and 1/4 chloroform were added to the supernatant collected in advance. After centrifugation at $12,000\times g$ at 4°C , 20 μL of 10 % SDS (Biosharp, Beijing, China) was added and repeatedly blown, and then loading buffer (TransGen Biotech, Beijing, China) was added for subsequent experiments.

A protein separation kit purchased from KeyGEN (Nanjing) was used to extract nucleic and cellular proteins. Quantitative proteins were dropped into 12 % sodium dodecyl sulfate polyacrylamide gel electrophoresis (SDS-PAGE) gel wells for electrophoresis and then transferred on PVDF membranes (Millipore, Germany), followed by closure with 5 % skimmed dry milk for 2 h and incubation with relative antibodies overnight. After washing with Tris buffered saline with tween (TBST), the membranes were incubated with HRP-labeled secondary antibodies for 1 h. After TBST washing again, the membrane was placed in a ChemiScope machine (Clinx, Shanghai) darkroom and imaged by adding drops of an equal mix of ECL reagent (Vazyme). Grayscale analysis of protein bands was completed using ImageJ software, and the data were standardized to GAPDH or histone H3.

2.8. Transmission electron microscopy observation

The kidney tissues removed by autopsy were washed with PBS to remove blood stains, cut into approximately 1 cm^3 pieces, placed in EP tubes, filled with 2.5 % glutaraldehyde and stored at 4°C . The pieces were then fixed, dehydrated, infiltrated, embedded, polymerized and sectioned to a thickness of 70 nm, dyed with uranyl acetate and lead citrate. Subsequently, the photos were captured for observation through an H-7650 (Hitachi, Tokyo, Japan).

2.9. Cell culture and cell viability assay

HK-2 cells were purchased from the Cell Bank of the Chinese Academy of Sciences (Shanghai) and cultivated in DMEM/F12 (Servicebio, Wuhan) with 10 % fetal bovine serum (Viva Cell BIOSCIENCES, Shanghai) and 1 % penicillin-streptomycin solution (Biosharp). The cells were maintained at 37°C in a humid environment of 5 % CO_2 . At the end of the drug treatment, DMEM/F12 containing 10 % CCK-8 was used and cultivated for 20 min. Subsequently, at 450 nm, absorption metrics were tested using a microplate reader (Bioteck) and substituted into the formula to calculate cell viability.

2.10. Immunofluorescence staining

Cells were inoculated in crawlers, first fixed with 4 % paraformaldehyde for half an hour after drug pretreatment, and then permeabilized in 0.2 % Triton X-100 for 12 min. Following washing with TBS, 5 % BSA was used to seal the cells for 2 h. Then, NLRP3 or apoptosis speck-like protein (ASC) primary antibodies were used for further incubation overnight at 4°C . All dilution ratios were 1:200. Subsequently, after a TBS wash, the cells were cultured with FITC-labeled secondary antibody (1:200) or Cy3-labeled secondary antibody (1:400) at 37°C for an hour under light-proof conditions. Then, the cells were counterstained with Hoechst 33,258. The cell crawl was inverted on a slide with a drop of sealer (BOSTER, Wuhan) and then placed in a wet box. Pictures

were acquired using a confocal microscope (Olympus, Shanghai).

2.11. Enzyme-linked immunosorbent assay (ELISA)

An ELISA detection kit (Thermo Scientific, United States) was used to detect the presence of inflammatory cytokines such as IL-1 β in the cell supernatants according to the manufacturer's instructions. Then, absorbance values were measured with a microplate reader. The concentration of IL-1 β was calculated by a relative standard curve and denoted by pg/mL.

2.12. ASC oligomerization assay

Cells were repeatedly blown using a 27-gauge needle in lysis solution (25 mM Na_3PO_4 , 187.5 mM NaCl, 25 mM HEPES and 125 mM NaHCO_3) along with proteinase inhibitor and then centrifuged for 5 min at $8000\times g$. The pellet was removed from the lysate and washed twice with PBS before being resuspended in 40 μL lysis solution and crosslinked for 30 min at 37°C using 2 mM disuccinimidyl suberate (DSS) (Sigma-Aldrich). After centrifugation at $8000\times g$ for 10 min, 20 μL SDS loading buffer was added to the pellets, which were boiled for 10 min for subsequent Western blot experiments.

2.13. Measurement of ROS levels

Intracellular ROS content was determined by a Reactive Oxygen Species Assay Kit (Wanleibio). Cells were first treated with 1 % t-butylhydroperoxide (TBHP) for 30 min at 37°C , followed by 20 min of treatment with 2', 7'-Dichlorodihydrofluorescein diacetate (DCFH-DA, 2 μM). Subsequently, the cells were rinsed twice with PBS to eliminate unattached probes. Then, the microplate reader scanned the plates at 488 nm and 525 nm.

2.14. MitoTracker red staining

The bioactive mitochondria in cells were detected by MitoTracker Red CMXRos (Beyotime). Briefly, the cells were cultured with MitoTracker Red reagent (200 nM) for 20 min, washed with TBS, Hanks balanced salt solution (Servicebio, Wuhan) was added to confocal culture dishes (Biosharp), and images were captured under a confocal microscope.

2.15. $\Delta\Psi\text{m}$ measurement

The mitochondrial membrane potential (MMP) was assayed by JC-1 (Solarbio). Briefly, the positive control carbonyl cyanide 3-chlorophenylhydrazone (CCCP) was added to the cells for 20 min. Then, all cells were loaded with JC-1 probes and scanned with a microplate reader. The excitation and emission wavelengths of the JC-1 signals were 490 nm and 530 nm, respectively, while the excitation and emission wavelengths of the JC-1 aggregates were 525 nm and 590 nm, respectively.

2.16. Mitochondrial isolation, total DNA extraction and mitochondrial DNA (mtDNA) copy number assay

A Cell Mitochondria Isolation Kit (Beyotime) was used to acquire the mitochondrial and cytoplasmic fractions of HK-2 cells. In detail, the cells were homogenized with mitochondrial isolation reagent along with phenylmethanesulfonyl fluoride for 30 s on ice and left for 15 min, followed by centrifugation at $11,000\times g$ and 4°C for 10 min. Then, the mitochondria were saved in storage solution.

Total DNA extraction from kidney tissue and HK-2 cells was completed according to the Mini Spin Kit for Global Genetic DNA Purity (Beyotime) in accordance with the instructions. By applying a NanoDrop2000 spectrophotometer, the DNA quantity and purification were evaluated.

Subsequently, 10 ng DNA was used to perform qPCR analysis to estimate mtDNA copy number. Nuclear beta-2 microglobulin (B2M) was utilized as a standard for the measurement of mtDNA copy number in HK-2 cells using the mitochondrial ND1 gene (mtND1). The mtDNA copy number for mouse tissues was measured using the mitochondrially encoded cytochrome *c* oxidase subunit 2 (COX2) and adjusted to the nuclear ribosomal protein s18 (Rps18). [Supplementary Table S1](#) contains the primer sequences utilized in the mtDNA test.

2.17. Immunoprecipitation (IP)

IP RIPA buffer (Biosharp) containing cocktail (Sangon) was used to lyse the cells for 30 min. The lysates were centrifuged at $12,000\times g$ for 10 min at 4 °C. The supernatant was collected, and the protein concentration was determined. A total of 500 µg protein was acquired from the supernatant and incubated with 1 µg primary antibody to form an immune complex at 4 °C overnight on a rotary shaker. Then, 40 µL of protein A/G agarose beads (Beyotime) was incubated with the samples at 4 °C for 3 h. After centrifugation at 2500 rpm for 5 min, for subsequent Western blot examination, the beads were boiled with SDS loading buffers for 10 min after being rinsed with TBS 5 times.

2.18. Molecular docking

The PGC-1 α protein structure 7E2E and drug small molecule

structure were both found at <https://pubchem.ncbi.nlm.nih.gov> and <https://www.rcsb.org>, respectively. Furthermore, AutoDock and PyMOL software were applied for molecular docking and visualization.

2.19. Statistical analysis

The mean \pm standard deviation (SD) was used to calculate the unpaired Student's *t*-test or one-way ANOVA followed by Tukey's post hoc analysis for all data, which were then displayed according to GraphPad Prism software. When $*P < 0.05$, $**P < 0.01$ and $***P < 0.001$, differences were deemed significant. At least three separate experiments were used to collect all of the data.

3. Results

3.1. Mv alleviated LPS-induced AKI in mice

To test the preliminary protective impact of Mv, a septic AKI model was created in mice. The serum BUN and Cr levels were elevated in the LPS stimulation group compared with those in the solvent-only control group ($P < 0.001$). However, both BUN and Cr levels were decreased after Mv pretreatment at medium and high doses ($P < 0.01$ or $P < 0.001$), illustrating that Mv alleviating LPS induced kidney function damage (Fig. 1A and B). H&E staining showed inflammatory cell infiltration, tubular lesions, glomerular atrophy and necrosis in the LPS

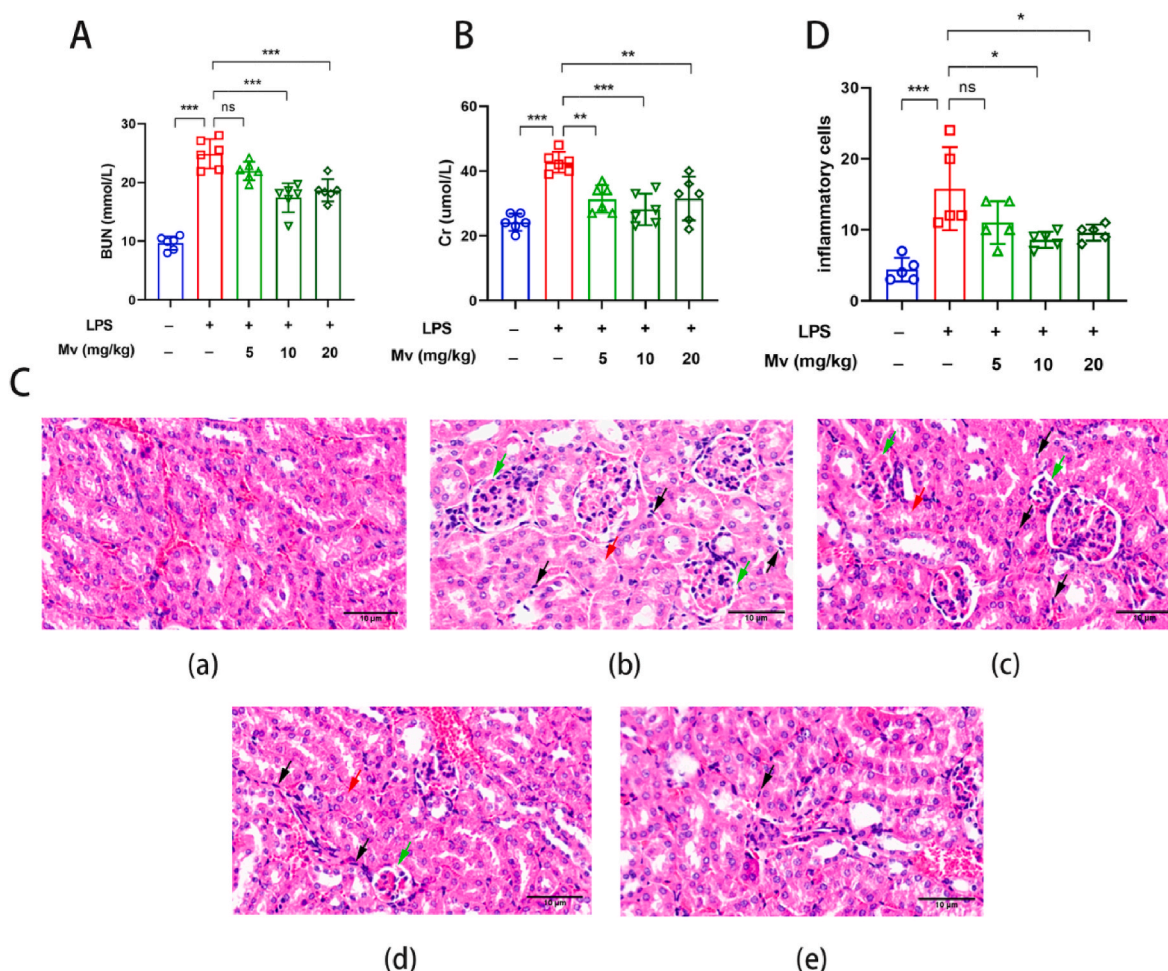


Fig. 1. The protective effects of Mv in LPS-induced AKI in mice. (A–B) Renal function markers: serum BUN and Cr. (C) Pictures of slices dyed with H&E (200 \times , scale bar: 10 µm). (D) Statistical analysis of inflammatory cells. Inflammatory cells are shown by black arrows, renal tubular lesions are shown by red arrows, and glomerular atrophy and necrosis are shown by green arrows. All statistics are displayed as the mean \pm SD. $**P < 0.01$, $***P < 0.001$, ns indicates no significant differences.

model group ($P < 0.001$), while medium and high doses of Mv pre-processing mitigated this pathological injury ($P < 0.05$) (Fig. 1C and D). In summary, Mv exerted a potentially protective role that prevented LPS from causing AKI *in vivo*.

3.2. Mv inhibited inflammatory cytokines and the NLRP3 inflammasome in mice

At the transcriptional level, Mv inhibited LPS-induced upregulation of pro-inflammatory cytokines of TNF- α , IL-1 β , IL-6 ($P < 0.001$), and down regulation of anti-inflammatory cytokine of IL-10 ($P < 0.001$) as well as upregulation of anti-inflammatory mediator of iNOS in the kidney tissues ($P < 0.001$), exhibiting sufficient anti-inflammatory bio-activities and may activate inflammasome with IL-1 β changes (Fig. 2A–E). Also, Mv reversed LPS induced M1 polarization and enhanced the M2 phenotype in mouse peritoneal macrophages (Supplementary Fig. 1). Next, we examined the impact of Mv on NLRP3 inflammasome activation. According to Western blotting analysis, pretreatment with Mv dramatically reduced LPS-induced the production of IL-1 β (p17) ($P < 0.001$) and caspase-1 (p20) ($P < 0.001$ for middle and high doses), as well as NLRP3 ($P < 0.001$) and ASC ($P < 0.05$, $P < 0.01$ or $P < 0.001$) in the kidney tissues (Fig. 2F–J). Overall, these findings indicated that in mice with LPS-induced AKI, Mv prevented proinflammatory cytokine production and NLRP3 inflammasome activation, alleviating inflammatory damage in the kidney.

3.3. Mv suppressed oxidative stress and enhanced Nrf2 expression in mice

Next, we investigated whether Mv could exert an antioxidant effect by controlling the level of oxidative stress *in vivo*. As shown in Fig. 3A–D, LPS-treated mice had higher MDA levels and reduced GSH-PX, SOD, and CAT levels when compared with those of normal mice ($P < 0.001$), which were all significantly corrected by Mv treatment in a dose-dependent manner ($P < 0.05$, $P < 0.01$ or $P < 0.001$) except for GSH-PX and CAT in the low dose group ($P > 0.05$). These data indicated that Mv reversed the imbalanced oxidative stress damage induced by LPS. Nrf2 increases the levels of endogenous antioxidants to mediate significant antioxidant activity [5]. Thus, we investigated whether Mv might control Nrf2 to reduce oxidative stress in AKI. As demonstrated in Fig. 3E–J, Mv increased the protein levels of Nrf2 and HO-1 ($P < 0.05$ or $P < 0.001$) and promoted the nuclear transfer of Nrf2 when compared to those of the model group ($P < 0.01$ or $P < 0.001$). All of these findings revealed that Mv could greatly boost antioxidant expression and increase Nrf2 protein levels in mice with LPS-induced AKI.

3.4. Mv blocked the activation of the NLRP3 inflammasome in HK-2 cells

We pretreated HK-2 cells with or without Mv and then activated the NLRP3 inflammasome with the activator ATP to assess the impact of Mv (Fig. 4). The CCK-8 test indicated that Mv had no effect on cell viability until 20 μ M ($P < 0.05$) (Fig. 4A). None of the concentrations of LPS showed any effect on cell viability within the range from 0.1 to 1000 μ g/mL ($P > 0.05$) (Fig. 4B). Pretreatment with Mv for 2 h and LPS/ATP costimulation for 24 h showed an effect on cell viability at

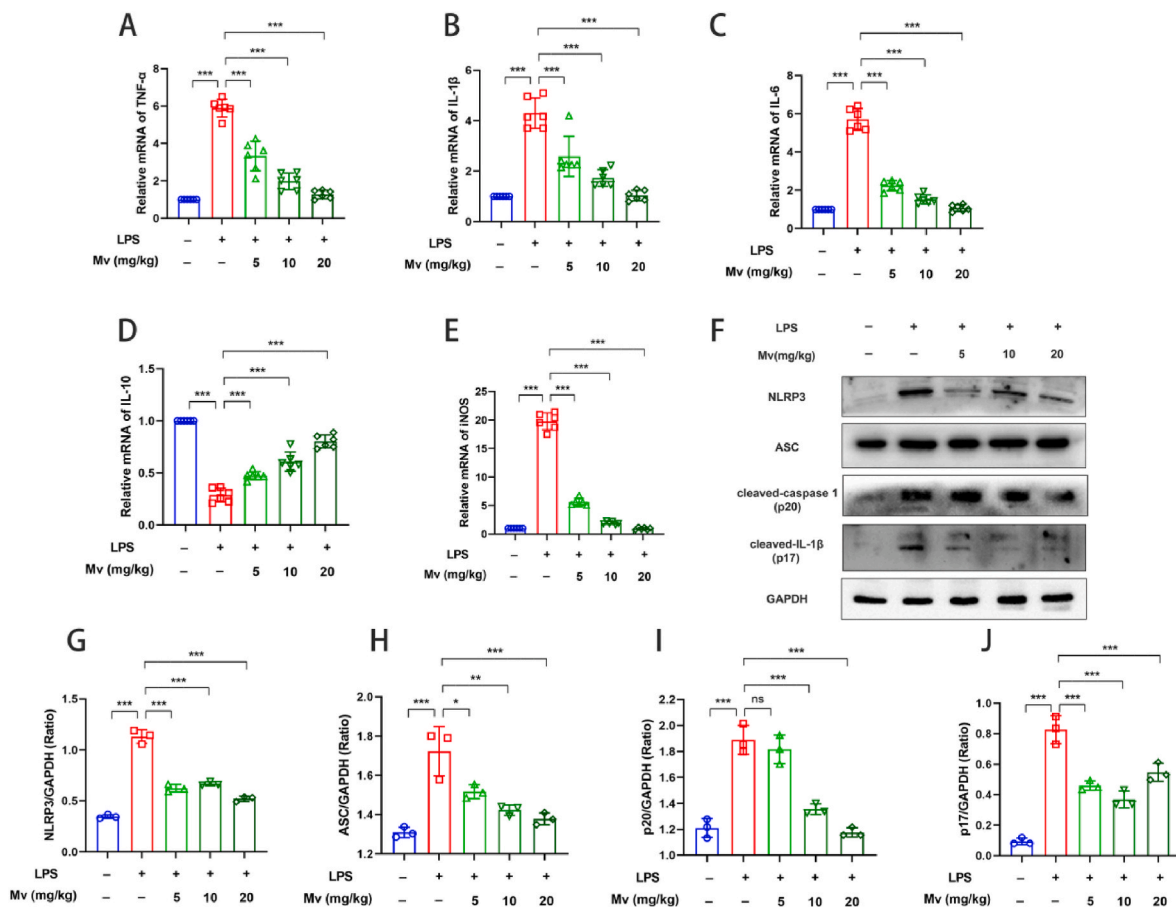


Fig. 2. In mice with LPS-induced AKI, Mv reduced inflammatory cytokine generation and NLRP3 inflammasome activation. (A–E) Proinflammatory and anti-inflammatory cytokine mRNA levels. (F) Images of NLRP3 inflammasome protein expression from the Western blot analysis. (G–J) Densitometric analysis of relevant proteins, and the internal reference was GAPDH. All data are presented as the means \pm SD. * $P < 0.05$, ** $P < 0.01$, *** $P < 0.001$, ns notes no significant differences.

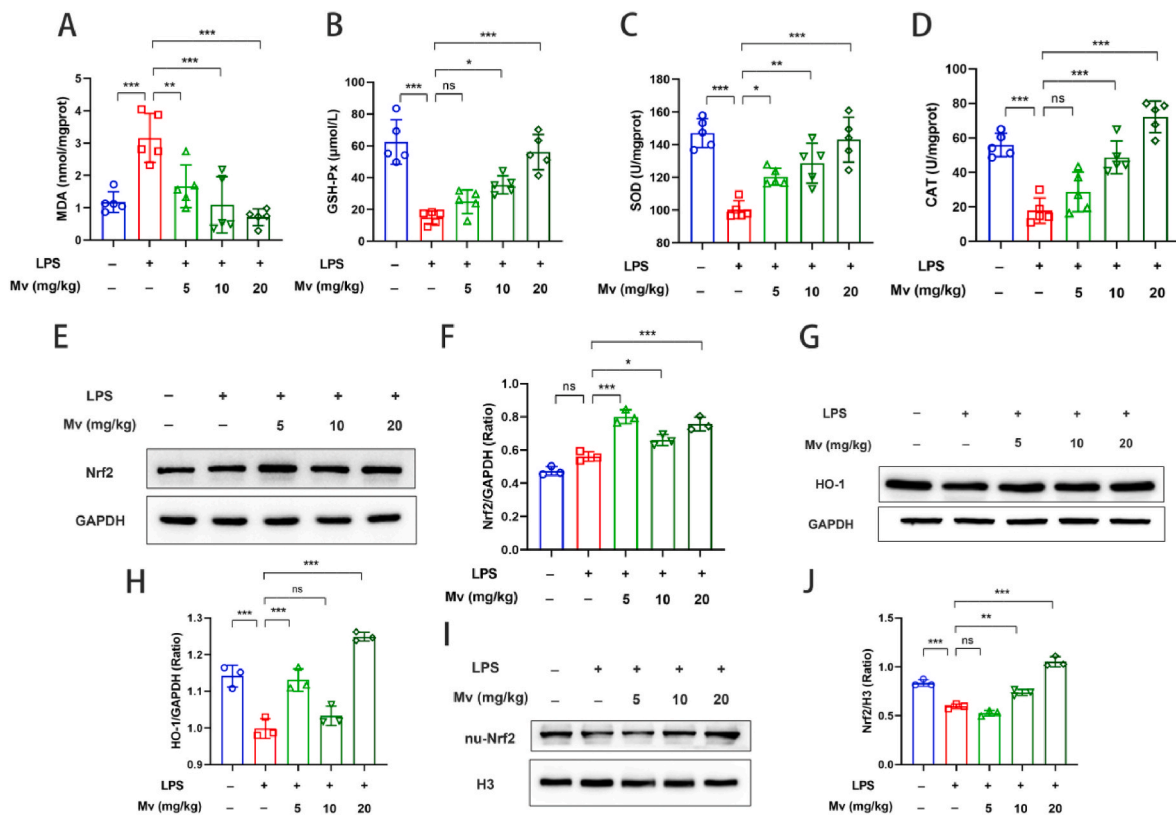


Fig. 3. Mv enhanced the antioxidative stress capacity and the protein level of the Nrf2 signaling pathway in mice with septic AKI. (A–D) With corresponding assay kits, indicators of lipid peroxidation and antioxidant activity were measured. (E, G, I) Western blot images of the protein levels of Nrf2, HO-1 and nuclear Nrf2. (F, H, J) Densitometric analysis of relevant proteins; the internal reference is GAPDH or H3. All data are presented as the means \pm SD. * $P < 0.05$, ** $P < 0.01$, *** $P < 0.001$, ns notes no significant differences.

concentrations of 50 μ M ($P < 0.05$) and 100 μ M ($P < 0.01$) (Fig. 4 C). Therefore, Mv at doses of 5, 10 and 20 was chosen for the follow-up study. Western blot results showed that in whole-cell lysates, pretreatment with Mv for 2 h inhibited NLRP3 inflammasome complex proteins, both including NLRP3 and ASC at 10 μ M dose ($P < 0.05$ or $P < 0.001$) (Fig. 4E and F). In the cell culture supernatant, Mv also significantly inhibited cleaved caspase-1 (p20) secretion ($P < 0.05$ or $P < 0.001$) (Fig. 4 G). In addition, ELISA showed that Mv decreased the release of cleaved IL-1 β (p17) caused by LPS plus ATP ($P < 0.001$) (Fig. 4 H). The above results suggested that Mv exerted a result consistent with that *in vivo*, namely, inhibition of NLRP3 inflammasome activation.

3.5. Mv attenuated mitochondrial dysfunction and improved mitochondrial biogenesis in HK-2 cells

Mitochondria are enriched in renal tubular epithelial cells and targeted to renal injury; thus, we explored exactly how Mv affects mitochondrial activity. The protective effect of Mv on MMP, which may be a reflection of mitochondrial homeostasis, was discovered using a JC-1 kit. When the MMP is higher, red fluorescence is produced as JC-1 accumulates in the mitochondrial matrix to form a polymer. When the MMP is lower, JC-1 forms green fluorescence as a monomer. Here, the relative ratios of red to green fluorescence quantified MMP. As shown in Fig. 5A, costimulation with LPS and ATP decreased the MMP ($P < 0.001$), which showed the same tendency as the positive control, CCCP ($P < 0.001$). However, Mv pretreatment alleviated this process ($P < 0.01$), thereby recovering mitochondria damage. The major locations of cellular energy metabolism, aerobic respiration and ROS generation occur in mitochondria [20]. In the present study, TBHP was used as a positive control for inducing ROS production. The assay revealed that LPS plus ATP enhanced the level of ROS ($P < 0.05$), while Mv

preprocessing decreased this level in a dose-dependent manner improving mitochondria function ($P < 0.05$ or $P < 0.01$) (Fig. 5 B). In mouse kidney tissues, after receiving a high dosage of Mv pretreatment, mtDNA copy number drastically dropped at 20 μ M dose ($P < 0.01$) after being greatly raised in the LPS model group ($P < 0.01$). In HK-2 cells, LPS/ATP stimulation displayed reduced mtDNA copy number ($P < 0.01$), while Mv treatment did not show any significant difference ($P > 0.05$) (Supplementary Fig. 2). Thus, the mitochondria and cytoplasm were isolated for further detection. In Fig. 5 C–D, the mtDNA copy number was reduced in mitochondria under the condition of LPS/ATP costimulation ($P < 0.01$), indicating that the mitochondria discharge mtDNA into the cytoplasm ($P < 0.01$). However, pretreatment with Mv reversed this trend ($P < 0.01$ or $P < 0.001$). Additionally, the MitoTracker red fluorescence signal was softer in the LPS/ATP group than in the vehicle group, whereas the mitochondrial mass was considerably increased by Mv treatment (Fig. 5 E). Furthermore, TEM showed mitochondrial lesions such as mitochondrial swelling, crista breakage and translucency in the kidneys of AKI mice, while the morphology of mitochondria and cristae was normalized after Mv treatment (Fig. 5 F). These data implied that Mv attenuated LPS induced kidney mitochondrial dysfunction.

PGC-1 α mediates mitochondrial biogenesis and mitochondrial energy homeostasis [21]. According to the Western blot results, LPS down-regulated the PGC-1 α levels in the HK-2 cells ($P < 0.001$) and exhibited no significant difference in the kidney tissues ($P > 0.05$), whereas this effect were reversed by Mv pretreatment in a dose-dependent manner both in the HK-2 cells ($P < 0.001$) and the kidney tissues ($P < 0.01$ at 10 and 20 μ M doses) (Fig. 6 A, C, D, G). Additionally, the expression of PGC-1 α in the nucleus showed a similar trend with that of total protein, namely LPS did not influence nucleus PGC-1 α (nu-PGC-1 α) expression ($P > 0.05$) but Mv obviously enhanced

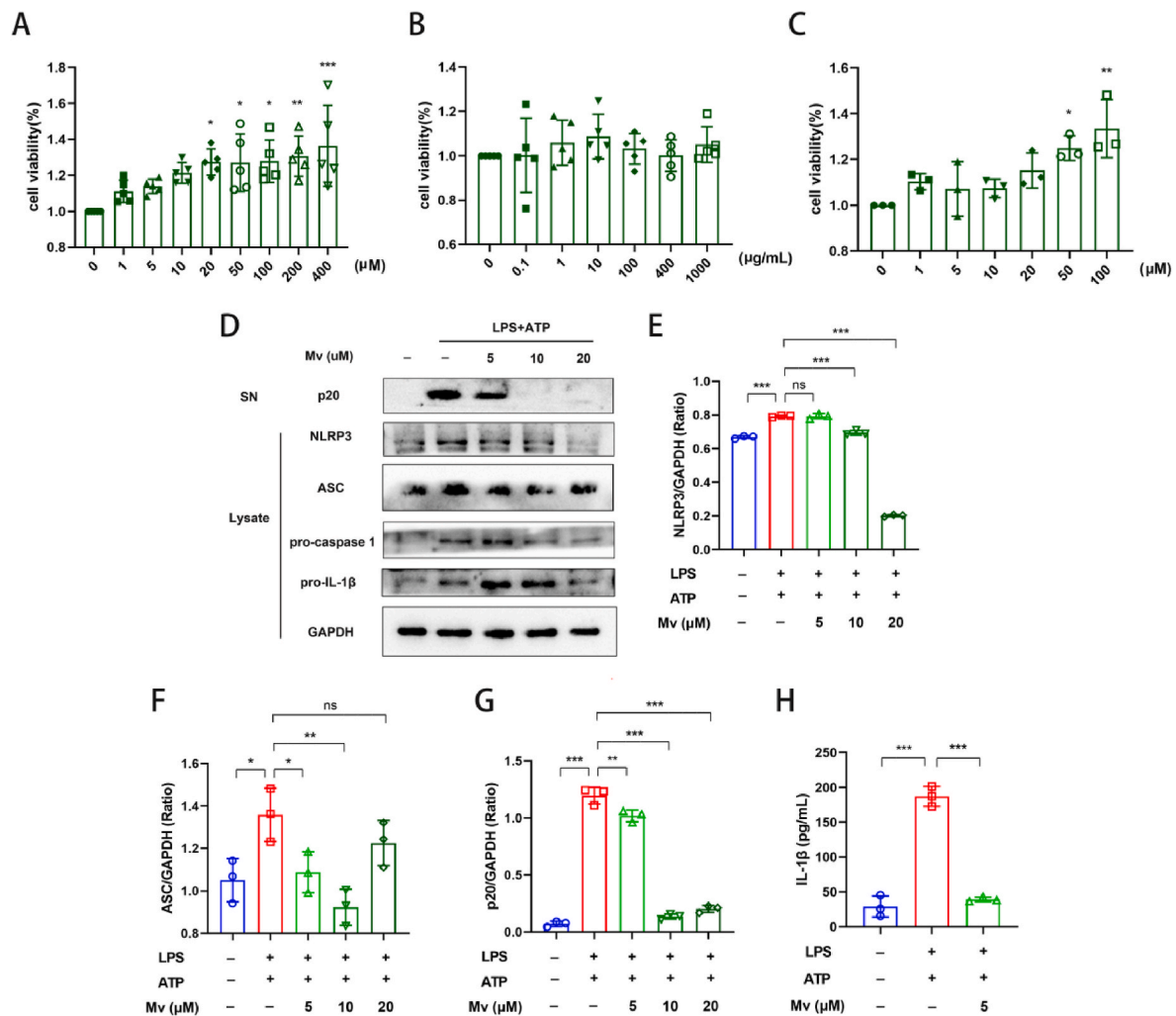


Fig. 4. Mv blocked NLRP3 inflammasome activation in HK-2 cells. (A) Cell viability following a 24-h pretreatment with various dosages of Mv. (B) Cell activity after 24 h of costimulation with various dosages of LPS and 1 mM ATP. (C) After pretreatment with various dosages of Mv for 2 h and then costimulation for 24 h with 10 μg/mL LPS and 1 mM ATP, cell viability was determined. (D) Images from a Western blot showing the NLRP3 inflammasome protein levels. (E–G) Densitometric analysis of relevant proteins, and the internal reference was GAPDH. (H) The IL-1β secretion level was measured with an ELISA test in the cell supernatant. All statistics are displayed as the mean ± SD. * $P < 0.05$, ** $P < 0.01$, *** $P < 0.001$, ns indicates no significant differences.

nu-PGC-1α levels ($P < 0.001$) (Fig. 6 B, E). Next, we validated the protein expression level of Nrf2 at the cellular level. As we expected, LPS/ATP costimulation reduced Nrf2 expression ($P < 0.05$), whereas this effect was rescued by Mv ($P < 0.001$), which exhibited the same trend as that *in vivo* (Fig. 6 A, F). These data fully verified that Mv improved mitochondrial biogenesis.

3.6. Mv inhibited NLRP3 inflammasome activation via the PGC-1α/Nrf2 signaling pathway

As presented in Fig. 7 A–C, the LPS/ATP-inhibited levels of Nrf2 and HO-1 were rescued after Mv treatment ($P < 0.001$), and this effect was abolished when PGC-1α was blocked with SR18292 ($P < 0.001$ or $P < 0.05$). To further confirm whether PGC-1α/Nrf2 is a key pathway by which Mv suppresses NLRP3 activation, SR18292 and ML385 were added to HK-2 cells, respectively. As we expected, SR18292 and ML385 treatment resulted in a reduction in the inhibitory effect of Mv on cleaved IL-1β ($P < 0.001$) (Fig. 7 D), ASC oligomerization (Fig. 7 E), ASC speck formation ($P < 0.001$ with ML385) (Fig. 7 F, H) and NLRP3 expression ($P < 0.05$ or $P < 0.01$) (Fig. 7 F, G). These inhibitors block assays data directly exhibited that PGC-1α/Nrf2 signaling pathway was involved in Mv mediated NLRP3 inflammasome inactivation in AKI *in*

vitro.

Next, we assayed the interaction of PGC-1α and Nrf2. The immunoprecipitation analysis showed that LPS/ATP diminished the affinity between these two proteins ($P < 0.001$), in contrast, Mv boosted PGC-1α binding to Nrf2 ($P < 0.001$) (Fig. 8 A and B). Interestingly, hydrogen bonding exists between PGC-1α and Mv (Fig. 8 C). These results collectively implied that the PGC-1α/Nrf2 pathway plays a key role in the inhibition of the NLRP3 inflammasome by Mv.

4. Discussion

A mouse septic AKI model was created *in vivo* using the LPS intraperitoneal injection method. Mv is a kind of anthocyanin with several medicinal advantages, such as anti-inflammatory and antioxidant properties. The statistical intake of anthocyanins is 200 mg/d [22]. A study investigated the bio-availability of anthocyanin from anthocyanin-rich juice in healthy young individuals between 23 and 27 years old and found that anthocyanin had a great beneficial for health via enhancing antioxidant properties [23]. However, its targets and underlying mechanisms in LPS-induced sepsis-related kidney injury remain to be explored. In this study, Mv attenuated the content of BUN and Cr, biomarkers of kidney injury, and improved histopathology,

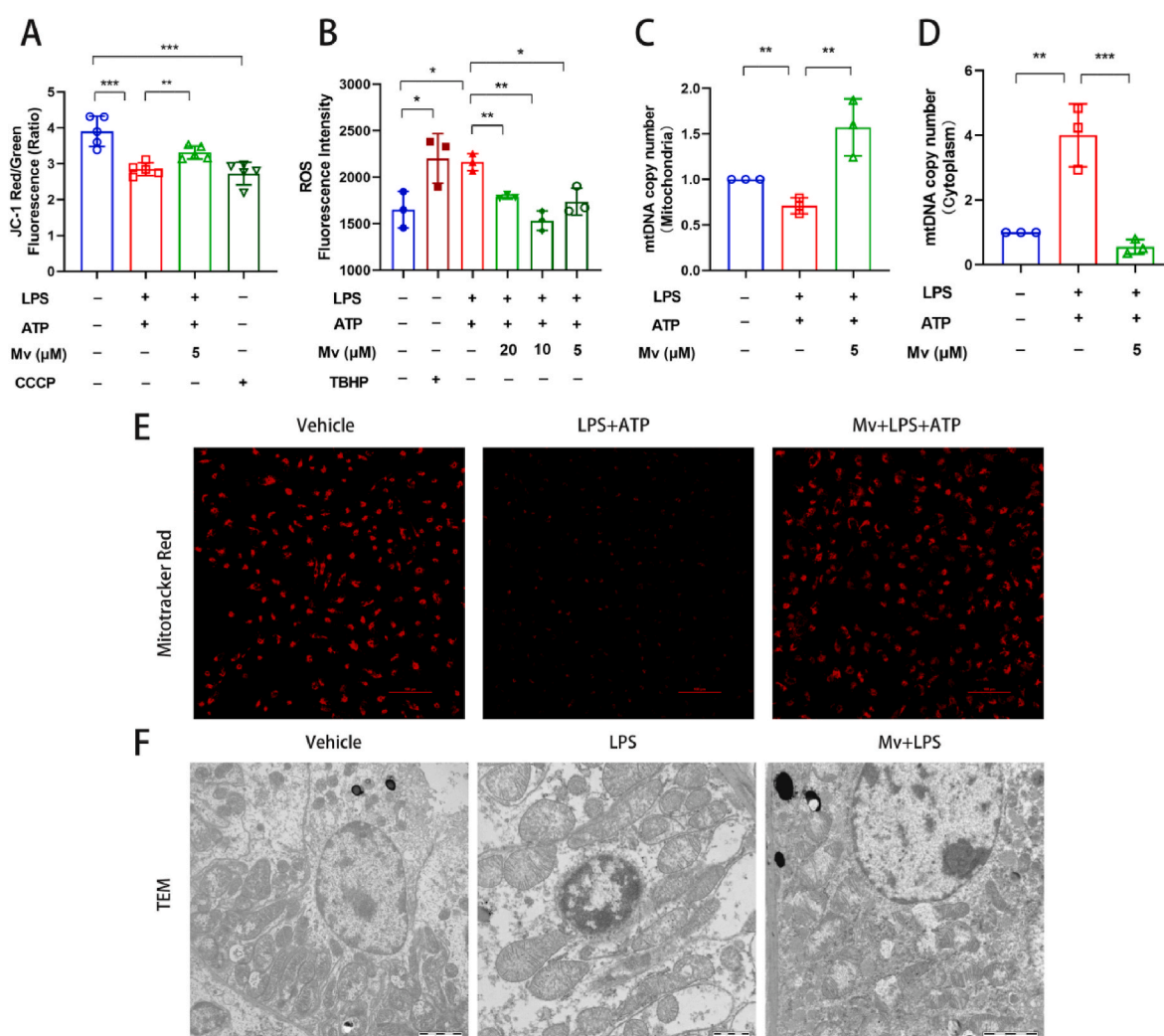


Fig. 5. Mv improved mitochondrial dysfunction in HK-2 cells. (A–B) MMP and the production of ROS were assayed by commercial kits. (C–D) mtDNA copy number was detected with RT–qPCR analysis in purified mitochondria and cytoplasm in HK-2 cells. (E) Immunofluorescence of mitochondria with MitoTracker red in HK-2 cells (scale bar: 100 px); the dose of Mv is 5 μM. (F) TEM ultrastructural observations of mitochondria in kidney tissues (scale bar: 2 μm); the dose of Mv was 20 mg/kg. All statistics are displayed as the mean ± SD. **P* < 0.05, ***P* < 0.01, ****P* < 0.001, ns indicates no significant differences.

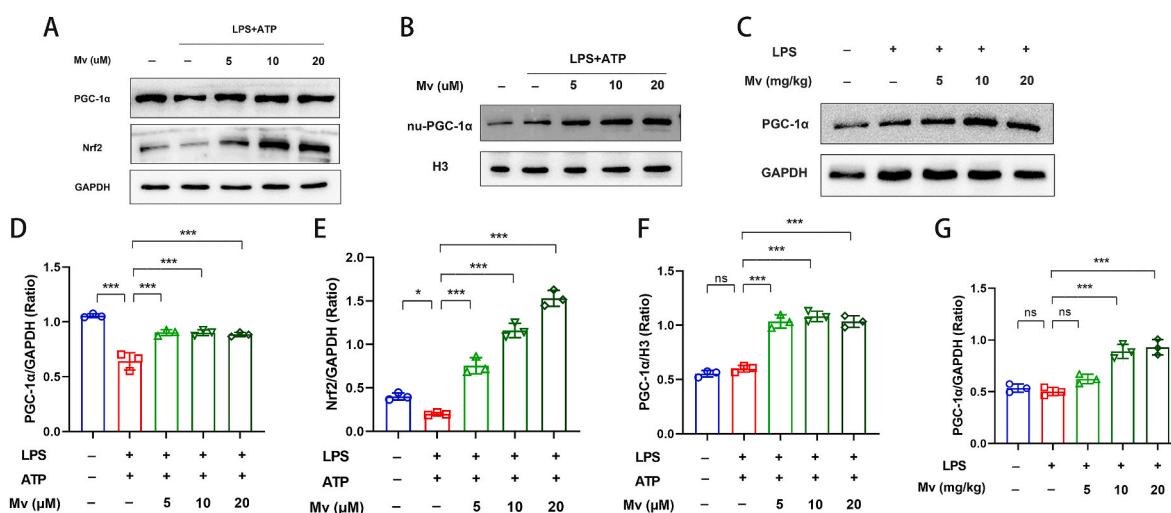


Fig. 6. PGC-1α and Nrf2 protein levels were increased under Mv treatment. (A–C) Western blot images of the protein levels of PGC-1α, nuclear PGC-1α and Nrf2 in HK-2 cells or kidney tissues. (D–G) Examination of relevant protein densitometry, and GAPDH or H3 was used as an internal reference. All statistics are displayed as the mean ± SD. **P* < 0.05, ****P* < 0.001, ns indicates no significant differences.

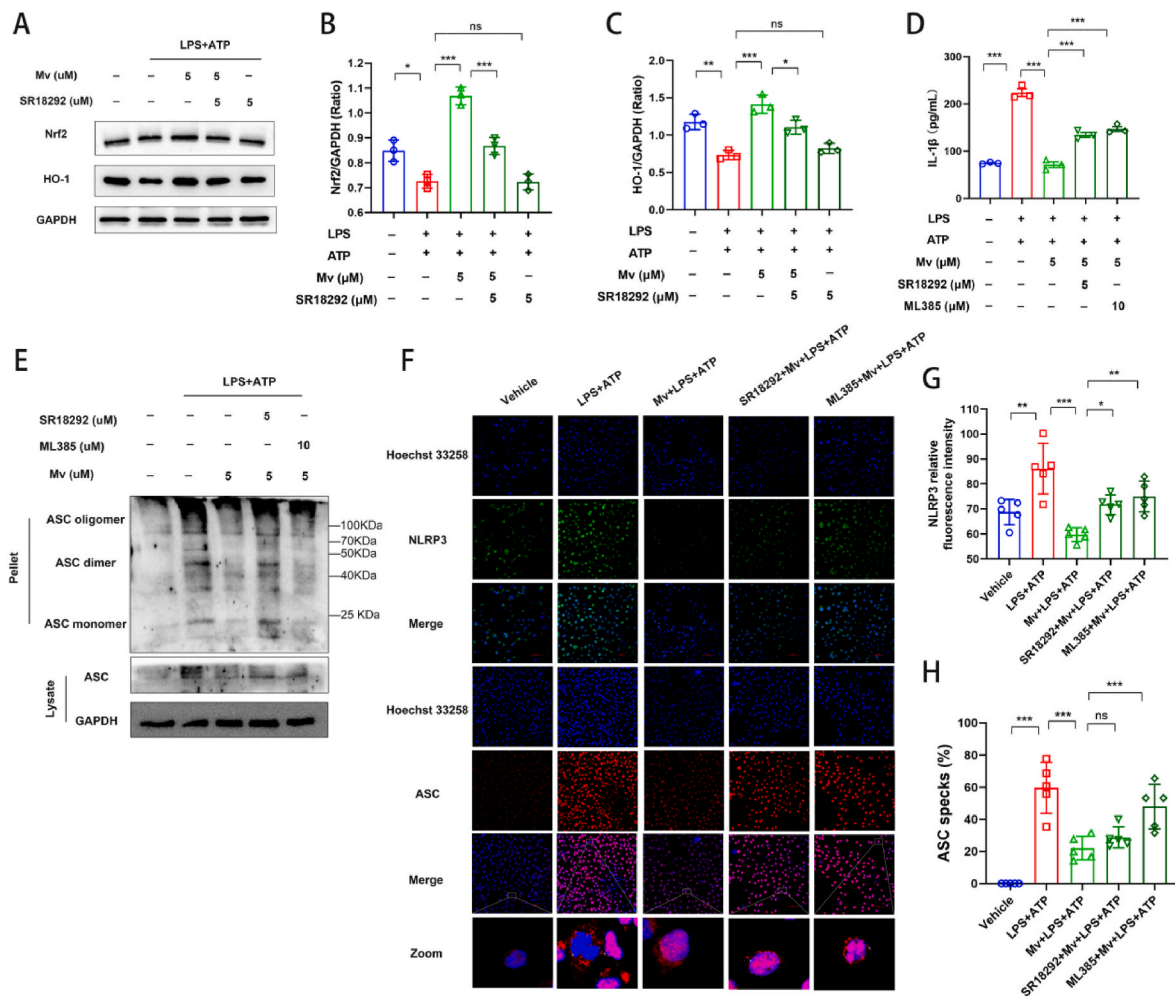


Fig. 7. Mv prevented NLRP3 inflammasome activation via the PGC-1 α /Nrf2 signaling pathway in HK-2 cells. (A) Western blot images of the protein levels of Nrf2 and HO-1 after pretreatment with SR18292 for 2 h followed by pretreatment with Mv for 2 h, followed by costimulation with LPS/ATP for 24 h. (B–C) Densitometric analysis of relevant proteins, and the internal reference was GAPDH. (D) IL-1 β production levels measured with an ELISA test in cell supernatant. (E) Western blot images of the protein levels of DSS-crosslinked ASC oligomers in pellets and ASCs in lysates in reaction buffer. (F) Immunofluorescence of NLRP3 and ASC (scale bar: 100 μ m). ASC speck formation is marked with white arrows. (G–H) Statistical analysis of NLRP3 fluorescence and ASC specks. All statistics are displayed as the mean \pm SD. * P < 0.05, ** P < 0.01, *** P < 0.001.

suggesting a potential protective effect of Mv in LPS-induced AKI. For the first time, the current study explored whether Mv inhibited NLRP3 inflammasome activation in sepsis AKI by regulating the PGC-1 α /Nrf2 signaling pathway *in vitro*. Our findings suggested that (1) Mv inhibited the NLRP3 inflammasome and oxidative stress both *in vitro* and *in vivo*; (2) Mv reduced mitochondrial dysfunction and promoted mitochondrial biogenesis; (3) Mv's inhibitory impact on NLRP3 inflammasome activation was regulated by the PGC-1 α /Nrf2 signaling pathway; and (4) Mv can facilitate the interaction between PGC-1 α and Nrf2.

When pathogenic microorganisms invade, the intrinsic immune system acts first, activating cytokines to release inflammatory mediators and clear exogenous pathogens. LPS is the main toxic component of gram-negative bacteria. In addition, LPS is a recognized PAMP that can activate TNF- α through the MAPK and NF- κ B pathways in sepsis [24]. In addition to Toll-like receptors located on the cell membrane, Nod-like receptors in the cytoplasm also recognize PAMPs or damage-associated molecular patterns [25]. The activated NLRP3 inflammasome promotes IL-1 β and IL-18 production and thus activates the downstream inflammatory response, which plays an essential role in sepsis [26–28]. Previous research revealed that suppression of the NLRP3 inflammasome could decrease iNOS levels [29,30]. In this study, Mv inhibited the expressions of the inflammatory cytokines such as TNF- α , IL-1 β , IL-6 and iNOS and increased the expression of the

anti-inflammatory cytokine IL-10. This validated the initial anti-inflammatory effect of Mv. Currently, NLRP3 is a candidate target for the treatment of sepsis. In addition to the inhibition of NLRP3 inflammasome expression exerted by Mv *in vivo*, to verify the regulatory role of Mv on the NLRP3 inflammasome in HK-2 cells, ATP was used to stimulate NLRP3 inflammasome activation. As expected, Mv also inhibited the NLRP3 inflammasome *in vitro* and suppressed the release of inflammatory cytokines. Additionally, in sepsis, the accumulation of constantly released inflammatory mediators affects the coupling process of the oxidative respiratory chain in mitochondria, causing the accumulation of ROS [31], which ultimately causes an unbalanced oxidative and antioxidant system in the body. Antioxidant enzymes, including SOD, GSH-PX, and CAT, are mediated by the Nrf2/ARE pathway, increasing cell resistance to chemical stimuli [32]. In line with expectations, Mv showed excellent antioxidant properties by enhancing these antioxidant enzyme activities and promoted the nuclear expression of Nrf2 and its downstream factor HO-1.

Given that abundant mitochondrial contents are enriched in the kidney, mitochondrial self-renewal through mitochondrial biogenesis is important for cellular energy metabolism. PGC-1 α , a mitochondrial biogenesis core molecule, has received much attention in the field of kidney injury research [33]. Under physiological conditions, mitochondria maintain intracellular homeostasis through quality control to

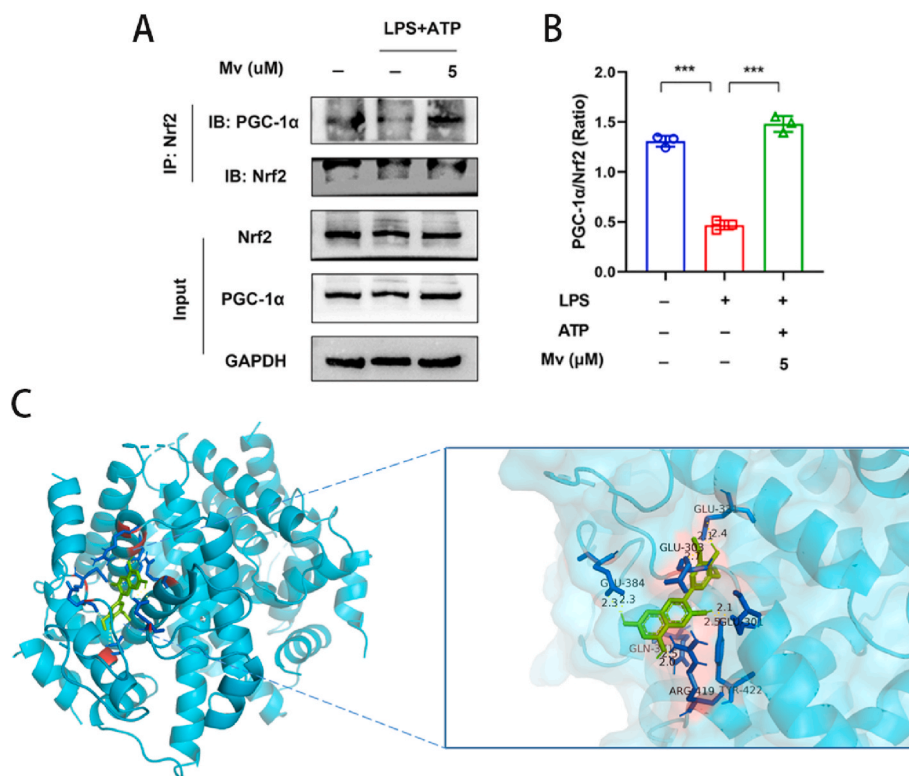


Fig. 8. Mv facilitated the interaction between PGC-1α and Nrf2 in HK-2 cells. (A) Cells were primed with Mv for 2 h and then stimulated for 24 h with LPS and ATP. Then, the PGC-1α to Nrf2 interaction was examined via immunoprecipitation. (B) Densitometric analysis of PGC-1α protein levels; the internal reference is GAPDH. All statistics are displayed as the mean \pm SD. *** $P < 0.001$. (C) Schematic representation of the molecular docking between Mv and PGC-1α. A hydrogen bond with ARG419 and the small molecule's hydroxyl O atom was created with a binding energy of -7.06 kcal/mol. Protein amino acid residues are shown in blue, whereas small molecule ligands are shown in green.

synthesize new mitochondria, maintain mitochondrial morphology and remove damaged mitochondria [6]. Under hazardous circumstances such as stress and hypoxia, mitochondrial quality control is disrupted, leading to structural damage and dysfunction, such as swelling, loss of cristae, decreased membrane potential, and an excessive amount of reactive oxygen radical production in the mitochondria, ultimately leading to tissue damage [34]. Our current results showed that Mv pretreatment reduced intracellular ROS accumulation, enhanced MMP and improved mitochondrial damage, thus maintaining mitochondrial homeostasis. And Mv pretreatment increased the expression levels of total PGC-1α proteins and nucleus PGC-1α. PGC-1α can be directly activated by AMPK and Sirt1 through phosphorylation and deacetylation and then coactivates the downstream transcription factor target Nrf1/2, which activates TFAM and combines with the initiation site of the subunit of the oxidative respiratory chain complex, thereby upregulating mtDNA replication and transcription [34,35]. Moreover, the NLRP3 inflammasome can be activated by abnormal mitochondria [28, 36], especially oxidative mitochondrial DNA, a secondary signal for NLRP3 inflammasome activation [23]. In the present study, we demonstrated that in HK-2 cells, LPS/ATP costimulation caused mtDNA transfer from mitochondria into the cytoplasm, while Mv treatment prohibited the discharge of mtDNA. Previous research has shown that PGC-1α protects against kidney fibrosis by inhibiting the NLRP3 inflammasome while maintaining mitochondrial viability [37]. Han and colleagues showed that PGC-1α attenuated neuroinflammation by inhibiting NLRP3 hyperactivation in microglia from mice after middle cerebral artery occlusion [10]. Additionally, in different models, high expression of Nrf2 inhibited NLRP3 inflammasome activation [5,9]. Thus, there is a strong relationship between mitochondrial biogenesis, oxidative stress and the NLRP3 inflammasome.

To further verify whether PGC-1α and Nrf2 regulate the effect of Mv

on NLRP3 inflammasome activation, inhibitor experiments were used to observe the crosstalk between signaling pathways. Interestingly, we found that SR18292 at a dose of 5 μM inhibited the protein expression of Nrf2 and its downstream transcription factor HO-1. Moreover, pretreatment with both SR18292 and ML385 significantly reversed the inhibition of IL-1β release by Mv, ASC oligomerization and ASC speckle-like formation. This finding demonstrated that Mv inhibited NLRP3 activation via the PGC-1α/Nrf2 signaling pathway. Furthermore, some data demonstrate that PGC-1α and Nrf2 have complementary roles [4] (Fig. 9). Therefore, we hypothesized that Nrf2 and PGC-1α work together to regulate the transcription of mitochondrial genes and then we observed evidence that Mv promoted the interaction of PGC-1α and Nrf2 via IP experiments. Although the present study demonstrated the protective effects of Mv against septic kidney injury in terms of oxidative stress, inflammation and mitochondrial function in *in vitro* and *in vivo*, the inflammatory state would be enriched by measuring more stable NO levels in the kidney and macrophages as well as the ROS levels in macrophages. Meanwhile, the influence of Mv on intestinal bacterial changes would also expand its effects in AKI, which is a significant limitation of this study.

5. Conclusions

Overall, Mv alleviated LPS-induced septic AKI, improved mitochondrial function, stimulated mitochondrial biogenesis, and inhibited the NLRP3 inflammasome via the PGC-1α/Nrf2 pathways. These findings suggest that Mv can be further applied in preclinical studies as a preventive target in septic acute kidney injury.

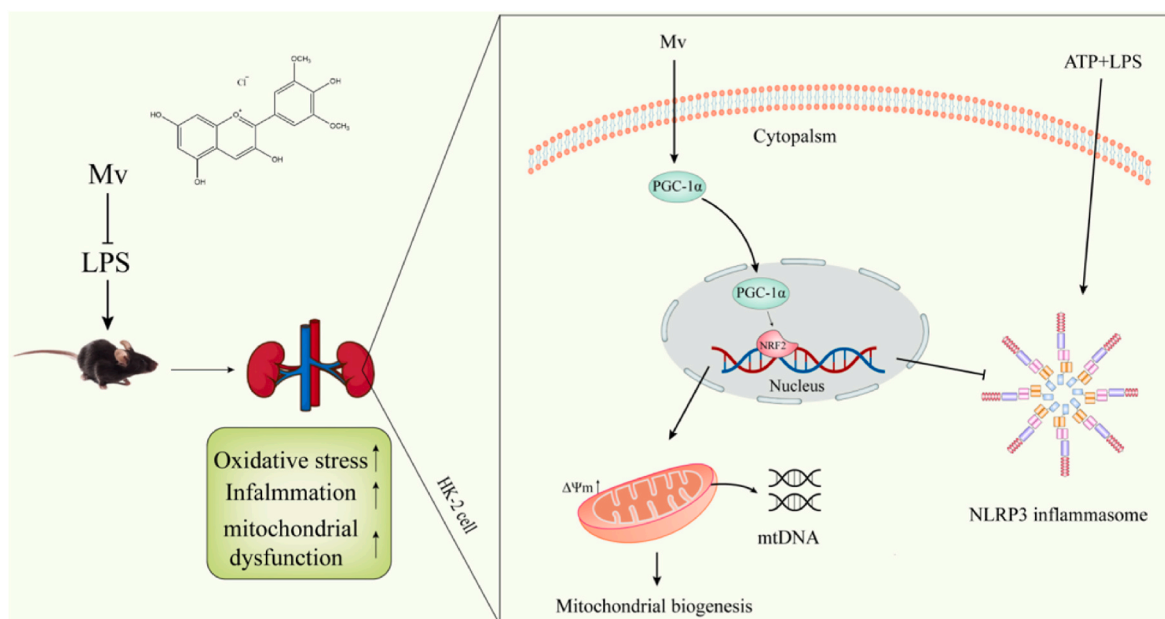


Fig. 9. Mechanistic illustration of Mv protection against septic AKI.

CRedit authorship contribution statement

Hui Fan: Writing – original draft, Software, Methodology, Data curation, Conceptualization. **Yong Sun:** Writing – original draft, Software, Methodology, Data curation, Conceptualization. **Xiao Zhang:** Visualization, Investigation. **Yao Xu:** Visualization, Investigation. **Yuanyuan Ming:** Validation, Software. **Le Zhang:** Validation, Software. **Panpan Zhao:** Writing – review & editing, Project administration, Funding acquisition.

Declaration of competing interest

The authors declare that they have no known competing financial interests or personal relationships that could have appeared to influence the work reported in this paper.

Data availability

For detailed data, please contact the corresponding author

Acknowledgement

The authors thank the Medical Research Project of Jiangsu Provincial Health Commission (No.H2023145), and the Jiangsu Science and Technology Association Youth Science and Technology Talent Lifting Project (No. TJ-2023-058) for financial support. The funders had no role in study design, data collection and analysis, decision to publish, or preparation of the manuscript.

Appendix A. Supplementary data

Supplementary data to this article can be found online at <https://doi.org/10.1016/j.cbi.2023.110850>.

References

- [1] K.V. Swanson, M. Deng, The NLRP3 inflammasome: molecular activation and regulation to therapeutics 19 (2019) 477–489.
- [2] C. Bime, T. Zhou, T. Wang, M.J. Slepian, J.G. Garcia, L. Hecker, Reactive oxygen species-associated molecular signature predicts survival in patients with sepsis, *Pulm. Circ.* 6 (2016) 196–201.
- [3] D.C. Cornelius, C.H. Baik, O.K. Travis, D.L. White, C.M. Young, W. Austin Pierce, C. A. Shields, B. Poudel, J.M. Williams, NLRP3 inflammasome activation in platelets in response to sepsis, *Phys. Rep.* 7 (2019), e14073.
- [4] H. Ma, C. Xie, Z. Chen, G. He, Z. Dai, H. Cai, H. Zhang, H. Lu, H. Wu, X. Hu, K. Zhou, G. Zheng, H. Xu, C. Xu, in: MFG-E8 Alleviates Intervertebral Disc Degeneration by Suppressing Pyroptosis and Extracellular Matrix Degradation in Nucleus Pulposus Cells via Nrf2/TXNIP/NLRP3 axis, vol. 8, 2022, p. 209.
- [5] T. Satoh, D. Trudler, C.K. Oh, S.A. Lipton, Potential therapeutic use of the rosemary diterpene carnosic acid for Alzheimer's disease, Parkinson's disease, and long-COVID through NRF2 activation to counteract the NLRP3 inflammasome, *Antioxidants* (2022) 11.
- [6] N. Arulkumaran, C.S. Deutschman, M.R. Pinsky, B. Zuckerbraun, P.T. Schumacker, H. Gomez, A. Gomez, P. Murray, J.A. Kellum, Mitochondrial function in sepsis, *Shock* 45 (2016) 271–281.
- [7] S.S. Dhar, S. Ongwijitwat, M.T.T. Wong-Riley, Nuclear respiratory factor 1 regulates all ten nuclear-encoded subunits of cytochrome c oxidase in neurons, *J. Biol. Chem.* 283 (2008) 3120–3129.
- [8] C.T. Campbell, J.E. Kolesar, B.A. Kaufman, Mitochondrial transcription factor A regulates mitochondrial transcription initiation, DNA packaging, and genome copy number, *Biochim. Biophys. Acta* 1819 (2012) 921–929.
- [9] B. Han, W. Jiang, P. Cui, K. Zheng, C. Dang, J. Wang, H. Li, L. Chen, R. Zhang, Q. M. Wang, Z. Ju, J. Hao, Microglial PGC-1α protects against ischemic brain injury by suppressing neuroinflammation 13 (2021) 47.
- [10] B.Y. Nam, J.H. Jhee, J. Park, S. Kim, in: PGC-1α Inhibits the NLRP3 Inflammasome via Preserving Mitochondrial Viability to Protect Kidney Fibrosis, vol. 13, 2022, p. 31.
- [11] A. Bastin, A. Sadeghi, The effects of malvidin on oxidative stress parameters and inflammatory cytokines in LPS-induced human, THP-1 cells 236 (2021) 2790–2799.
- [12] Y. Ma, Y. Li, H. Zhang, Y. Wang, C. Wu, Malvidin induces hepatic stellate cell apoptosis via the endoplasmic reticulum stress pathway and mitochondrial pathway 8 (2020) 5095–5106.
- [13] T. Dai, K. Shi, G. Chen, Y. Shen, T. Pan, Malvidin attenuates pain and inflammation in rats with osteoarthritis by suppressing NF-κB signaling pathway, *Inflamm. Res.* 66 (2017) 1075–1084.
- [14] H. Fan, J. Cui, F. Liu, W. Zhang, H. Yang, N. He, Z. Dong, J. Dong, Malvidin protects against lipopolysaccharide-induced acute liver injury in mice via regulating Nrf2 and NLRP3 pathways and suppressing apoptosis and autophagy, *Eur. J. Pharmacol.* 933 (2022), 175252.
- [15] X. Liu, F. Zheng, S. Li, Z. Wang, X. Wang, L. Wen, Y. He, Malvidin and its derivatives exhibit antioxidant properties by inhibiting MAPK signaling pathways to reduce endoplasmic reticulum stress in ARPE-19 cells, *Food Funct.* 12 (2021) 7198–7213.
- [16] F.L. Fagundes, Q.C. Pereira, M.L. Zarricueta, R.C. Dos Santos, in: Malvidin Protects against and Repairs Peptic Ulcers in Mice by Alleviating Oxidative Stress and Inflammation, vol. 13, 2021.
- [17] P. Zhao, X. Li, Q. Yang, Y. Lu, G. Wang, H. Yang, J. Dong, H. Zhang, Malvidin alleviates mitochondrial dysfunction and ROS accumulation through activating AMPK-α/UCP2 axis, thereby resisting inflammation and apoptosis in SAE mice, *Front. Pharmacol.* 13 (2022), 1038802.
- [18] B. Salehi, J. Sharifi-Rad, F. Cappellini, Z. Reiner, D. Zorzan, M. Imran, B. Sener, M. Kilic, M. El-Shazly, N.M. Fahmy, E. Al-Sayed, M. Martorell, C. Tonelli, K. Petroni, A.O. Docea, D. Calina, A. Maroyi, The therapeutic potential of

- anthocyanins: current approaches based on their molecular mechanism of action, *Front. Pharmacol.* 11 (2020).
- [19] W. Ma, S. Ao, J. Zhou, J. Li, X. Liang, X. Yang, H. Zhang, B. Liu, W. Tang, H. Liu, H. Xiao, H. Liang, X. Yang, Methylsulfonylmethane protects against lethal dose MRSA-induced sepsis through promoting M2 macrophage polarization, *Mol. Immunol.* 146 (2022) 69–77.
- [20] J. Sun, J. Zhang, J. Tian, G.M. Virzi, K. Digvijay, L. Cueto, Y. Yin, M.H. Rosner, C. Ronco, Mitochondria in sepsis-induced AKI, *J. Am. Soc. Nephrol.* 30 (2019) 1151–1161.
- [21] S.Y. Li, K. Susztak, The role of peroxisome proliferator-activated receptor γ coactivator 1 α (PGC-1 α) in kidney disease, *Semin. Nephrol.* 38 (2018) 121–126.
- [22] S. Kuntz, S. Rudloff, H. Asseburg, C. Borsch, B. Fröhling, F. Unger, S. Dold, B. Spengler, A. Römpp, C. Kunz, Uptake and bioavailability of anthocyanins and phenolic acids from grape/blueberry juice and smoothie in vitro and in vivo, *Br. J. Nutr.* 113 (2015) 1044–1055.
- [23] R. Zamora-Ros, V. Knaze, L. Luján-Barroso, N. Slimani, I. Romieu, M. Touillaud, R. Kaaks, B. Teucher, A. Mattiello, S. Gironi, F. Crowe, H. Boeing, J. Förster, J. R. Quirós, E. Molina, J.M. Huerta, D. Engeset, G. Skeie, A. Trichopoulou, V. Dilis, K. Tsiotas, P.H.M. Peeters, K.-T. Khaw, N. Wareham, B. Bueno-de-Mesquita, M. C. Ocké, A. Olsen, A. Tjønneland, R. Tumino, G. Johansson, I. Johansson, E. Ardanaz, C. Sacerdote, E. Sonestedt, U. Ericson, F. Clavel-Chapelon, M.-C. Boutron-Ruault, G. Fagherazzi, S. Salvini, P. Amiano, E. Riboli, C.A. González, Estimation of the intake of anthocyanidins and their food sources in the European Prospective Investigation into Cancer and Nutrition (EPIC) study, *Br. J. Nutr.* 106 (2011) 1090–1099.
- [24] H. Liu, W. Zhang, S. Dong, L. Song, S. Zhao, C. Wu, X. Wang, F. Liu, J. Xie, J. Wang, Y. Wang, Protective effects of sea buckthorn polysaccharide extracts against LPS/d-GalN-induced acute liver failure in mice via suppressing TLR4-NF- κ B signaling, *J. Ethnopharmacol.* 176 (2015) 69–78.
- [25] N. Kelley, D. Jeltama, Y. Duan, Y. He, The NLRP3 inflammasome: an overview of mechanisms of activation and regulation, *Int. J. Mol. Sci.* 20 (2019).
- [26] E. Latz, T.S. Xiao, A. Stutz, Activation and regulation of the inflammasomes, *Nat. Rev. Immunol.* 13 (2013) 397–411.
- [27] A. Babelova, K. Moreth, W. Tsalastra-Greul, J. Zeng-Brouwers, O. Eickelberg, M. F. Young, P. Bruckner, J. Pfeilschifter, R.M. Schaefer, H.J. Gröne, L. Schaefer, Biglycan, a danger signal that activates the NLRP3 inflammasome via toll-like and P2X receptors, *J. Biol. Chem.* 284 (2009) 24035–24048.
- [28] A. Vilaysane, J. Chun, M.E. Seamone, W. Wang, R. Chin, S. Hirota, Y. Li, S.A. Clark, J. Tschoop, K. Trpkov, B.R. Hemmelgarn, P.L. Beck, D.A. Muruve, The NLRP3 inflammasome promotes renal inflammation and contributes to CKD, *J. Am. Soc. Nephrol.* 21 (2010) 1732–1744.
- [29] F. Liu, Z. Li, X. He, H. Yu, J. Feng, Ghrelin attenuates neuroinflammation and demyelination in experimental autoimmune encephalomyelitis involving NLRP3 inflammasome signaling pathway and pyroptosis, *Front. Pharmacol.* 10 (2019) 1320.
- [30] L. Hou, Y. Ye, H. Gou, H. Tang, Y. Zhou, X. Xu, Y. Xu, A20 inhibits periodontal bone resorption and NLRP3-mediated M1 macrophage polarization, *Exp. Cell Res.* 418 (2022), 113264.
- [31] S. Vera, R. Martínez, J.G. Gormaz, A. Gajardo, F. Galleguillos, R. Rodrigo, Novel relationships between oxidative stress and angiogenesis-related factors in sepsis: new biomarkers and therapies, *Ann. Med.* 47 (2015) 289–300.
- [32] T.B. Deramaut, C. Dill, M. Bonay, Regulation of oxidative stress by Nrf2 in the pathophysiology of infectious diseases, *Med. Maladies Infect.* 43 (2013) 100–107.
- [33] Y. Xu, J.A. Kabba, W. Ruan, Y. Wang, S. Zhao, X. Song, L. Zhang, J. Li, T. Pang, The PGC-1 α activator ZLN005 ameliorates ischemia-induced, Neuronal Injury In Vitro and In Vivo 38 (2018) 929–939.
- [34] N. Baker, J. Patel, M. Khacho, Linking mitochondrial dynamics, cristae remodeling and supercomplex formation: how mitochondrial structure can regulate bioenergetics, *Mitochondrion* 49 (2019) 259–268.
- [35] L.D. Popov, Mitochondrial biogenesis: an update, *J. Cell Mol. Med.* 24 (2020) 4892–4899.
- [36] J.W. Yu, M.S. Lee, Mitochondria and the NLRP3 inflammasome: physiological and pathological relevance, *Arch Pharm. Res. (Seoul)* 39 (2016) 1503–1518.
- [37] A. Khader, W.L. Yang, M. Kunczewitch, A. Jacob, J.M. Prince, J.R. Asirvatham, J. Nicastro, G.F. Coppa, P. Wang, Sirtuin 1 activation stimulates mitochondrial biogenesis and attenuates renal injury after ischemia-reperfusion, *Transplantation* 98 (2014) 148–156.